Polymeric filament thinning and breakup in microchannels

P. E. Arratia,[1,*] J. P. Gollub,[1,2] and D. J. Durian[1]
[1]*Department of Physics and Astronomy, University of Pennsylvania, Philadelphia, Pennsylvania 19104, USA*
[2]*Department of Physics, Haverford College, Haverford, Pennsylvania 19041, USA*
(Received 18 March 2007; revised manuscript received 4 February 2008; published 18 March 2008)

The effects of elasticity on filament thinning and breakup are investigated in microchannel cross flow. When a viscous solution is stretched by an external immiscible fluid, a low 100 ppm polymer concentration strongly affects the breakup process, compared to the Newtonian case. Qualitatively, polymeric filaments show much slower evolution, and their morphology features multiple connected drops. Measurements of filament thickness show two main temporal regimes: flow- and capillary-driven. At early times both polymeric and Newtonian fluids are flow-driven, and filament thinning is exponential. At later times, Newtonian filament thinning crosses over to a capillary-driven regime, in which the decay is algebraic. By contrast, the polymeric fluid first crosses over to a second type of flow-driven behavior, in which viscoelastic stresses inside the filament become important and the decay is again exponential. Finally, the polymeric filament becomes capillary-driven at late times with algebraic decay. We show that the exponential flow thinning behavior allows a measurement of the extensional viscosities of both Newtonian and polymeric fluids.

DOI: 10.1103/PhysRevE.77.036309 PACS number(s): 47.50.−d, 47.55.df, 83.50.Jf

I. INTRODUCTION

The progressive breakup of an initially stable fluid thread into small drops or bubbles is a rich phenomenon of great interest [1]. For example, flow focusing in microfluidic devices can continuously produce drops or bubbles whose sizes are controlled by the relative flow rate of the two immiscible fluids [2–7]. While most such work concerns Newtonian fluids, many fluids of interest for laboratory-on-a-chip applications are likely to exhibit complex microstructure and non-Newtonian behavior, such as viscoelasticity. Furthermore, viscoelastic effects, which can be quantified by the elasticity number $\mathrm{El}=\lambda\eta/(\rho L^2)$, scale inversely with the square of the device length scale (L) and are likely to be accentuated in microfluidic devices. Here, λ is the fluid relaxation time, η is viscosity, and ρ is density. For polymeric drop breakup in macroscopic flow, elasticity can give rise to breakup behavior that is markedly different from that of Newtonian fluids [8–11]. For example, a viscoelastic filament quiescent bath [12] undergoes an initial viscous-capillary regime in which the decrease in the filament diameter is linear, followed by a slower thinning process in which capillary forces are balanced by the fluid elastic stresses.

Recently, a numerical investigation in a flow-focusing device [13] showed qualitative differences with respect to Newtonian fluids such as prolonged thinning of the fluid filament and delay of drop pinch-off. No measurements of thinning rates or breakup times were presented. An experimental investigation in a "T" shaped geometry using a low viscosity, elastic fluid [14] also found prolonged thinning of the fluid filament. The authors observed a linear decrease in filament diameter followed by a "self-thinning" exponential regime, which was argued to have a rate inversely proportional to the fluid relaxation time (λ). However, λ was found to vary over an order of magnitude with shear rate, though it should remain constant. While both investigations found similar qualitative trends, no quantitative connection has yet been made to the extensional flow within the filament during thinning and breakup.

In this paper, we compare the filament thinning and breakup of Newtonian and viscoelastic fluids of equal shear viscosity in a microchannel cross-slot geometry. Here, the outer Newtonian fluid stretches the inner Newtonian or polymeric fluid into a thin filament until it eventually breaks up into drops. This geometry allows for very fine control of the flows over a broad range of shear rates. Measurements of filament thickness show two temporal regimes: (i) a flow-driven regime in which the filament thins exponentially and (ii) a capillary-driven regime in which the filament thins algebraically. Our analysis leads to a method of measuring the steady extensional viscosities of both Newtonian and polymeric fluids.

II. METHODS

The experimental configuration is a cross-slot microchannel, $W=50$ μm wide and $L=30$ μm deep, molded in poly(dimethylsiloxane) (PDMS, Dow Sylgard 184) using standard soft-lithography methods [15,16]. Channels are sealed with a glass cover slip after exposure to an oxygen plasma. In order to keep the microchannel wetting properties uniform, the glass cover slip is coated with a thin layer of PDMS prior to the exposure. The assembled channels are then baked for 12 h at 100 °C in order to obtain hydrophobic walls wetted by the continuous outer liquid phase.

The outer continuous phase is mineral oil containing 0.1% by weight of surfactant (SPAN 80, Fluka). Both Newtonian and polymeric fluids are used for the inner (or "dispersed") phase. The Newtonian fluid is a 90%-glycerin aqueous solution. The polymeric fluid is made by adding 100 ppm of high molecular weight polyacrylamide (PAA, $M_W=18\times10^6$, 15% polydispersity), which has a flexible backbone, to a Newton-

*Currently at the Department of Mechanical Engineering, University of Pennsylvania, Philadelphia, PA 19104, USA.

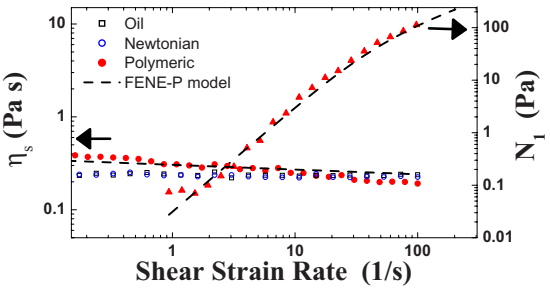

FIG. 1. (Color online) Fluid rheological characterization. (Left y axis) Shear viscosity vs shear strain rate for all fluids; oil =mineral oil; Newtonian=water-glycerin mixture; polymeric =PAA in water-glycerin mixture. The shear viscosity is nearly constant even for the polymeric solution $\eta_s \approx 0.24$ Pa s. (Right y axis) First normal stress difference for the polymeric solution vs shear strain rate. Dashed curves represent fits using the FENE-P model with parameters $\lambda=0.45$ s and $b=4500$.

ian 85%-glycerin aqueous solution with a measured shear viscosity of $\eta_{s,solv}=0.2$ Pa s; the water-glycerin mixture is used as a solvent for the polymer. It is dilute, below the overlap concentration of approximately 350 ppm. The interfacial tension between the continuous and dispersed phases is $\sigma=10$ mN/m. The fluids are characterized with a stress-controlled rheometer at 25 °C. As shown in Fig. 1, the shear viscosities of the oil and Newtonian fluids are nearly identical and independent of shear strain rate: $\eta_s \approx 0.24$ Pa s. Also as shown, the viscoelastic polymeric fluid exhibits nearly constant shear viscosity (power law index=0.97) and a first normal stress difference N_1, which increases quadratically with shear strain rate.

We fit the polymeric fluid shear rheology data to the widely used finite extensibility nonlinear elastic model with Peterlin's closure (FENE-P) [17–19]. In this model the fluid total stress tensor τ is assumed to be the sum of a contribution from the solvent and another resulting from the presence of polymer molecules such that $\tau=\tau_{solv}+\tau_{poly}$. The solution shear viscosity η_s is then the sum of the solvent and polymeric parts $\eta_s=\eta_{s,solv}+\eta_{s,poly}$. The FENE-P model is well-adapted for dilute (and semidilute) high molecular weight polymeric solutions and has been used previously to analyze filament thinning of polymeric fluids in macroscopic experiments [9]. A fluid described by the FENE-P model possesses the same dynamical properties as a fluid described by the much simpler Oldroyd-b model [18], which assumes that polymers can be modeled as Hookean springs. The main difference is that the Oldroyd-b model allows for infinite extension of polymer molecules, while the FENE-P model uses a spring-force law in which the polymer molecules can be stretched only by a finite amount in the flow field [17,18].

A simultaneous fit (Fig. 1) of the polymeric fluid η_s and N_1 data to the FENE-P model provides the fluid relaxation time λ and a dimensionless finite extensibility parameter b, which are the only two adjustable parameters [18]. The best fit results in $\lambda=0.45$ s and $b=4500$. Further details on the equations and methods used to fit the FENE-P model to the shear rheology can be found elsewhere [20].

The dispersed and continuous phases are injected into the central and side arms of the cross-channel, respectively, us-

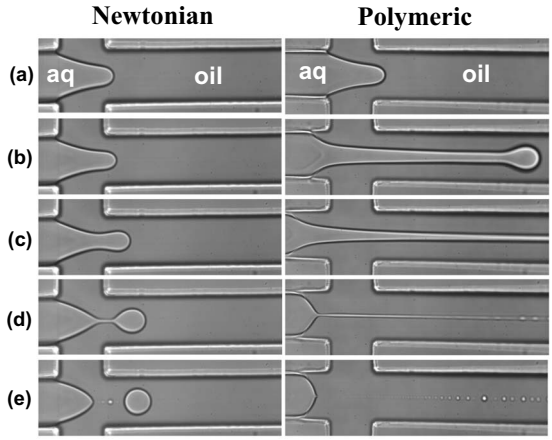

FIG. 2. Evolution of the thinning process for Newtonian (left column) and polymeric fluids (right column) for a flow rate ratio $q=Q_{oil}/Q_{aq}=60$, where Q_{oil}/Q_{aq} corresponds to the ratio of oil and aqueous phase flow rates. Oil is the continuous (outer) phase while the aqueous phase is either Newtonian or polymeric. (a) Initial regime; (b) $t/t_b=0.15$, where t_b is breakup time; (c) $t/t_b=0.45$; (d) $t/t_b=0.95$; and (e) after breakup. Values of t_b for the Newtonian and polymeric cases are 11.5 and 245 ms, respectively. Note the appearance of satellite droplets in the Newtonian case and multiple beads attached to the filament in the polymeric case [(d) and (e)]. The channel width and depth are 50 and 30 μm, respectively.

ing syringe pumps (Harvard Instruments). Experiments are performed for flow rate ratios, $q=Q_{oil}/Q_{aq}$, ranging from 10 to 200. In all cases, the aqueous flow rate is kept constant at $Q_{aq}=0.01$ l/min. This is low enough that the behavior is quasistatic, such that the periodicity—but not the morphology—depends on Q_{aq}. For this range of parameters, the Reynolds number is less than 0.01; therefore viscous forces are much larger than inertial forces. The capillary number Ca ranges from 1.25 to 50; therefore surface forces are larger than viscous forces. Under these conditions an aqueous filament is formed and stretched by the flow of the surrounding oil. The thinning and breakup of the filament are imaged using an inverted microscope and a fast video camera, with frame rates between 1 and 10 kHz.

III. OBSERVATIONS

A. Qualitative

Sample frames from video data are shown in Fig. 2, for both Newtonian and polymeric fluids, at a flow rate ratio of $q=60$. The Newtonian case, shown in the *left column*, displays typical filament thinning and drop formation. The aqueous phase is drawn into the cross-slot channel (a), and begins to elongate and collapse (b)–(d), forming a primary drop connected to a very thin filament; later (e) the filament thins at a faster rate and breaks into a large primary drop and small satellite droplets.

The polymeric case, shown in the *right column* of Fig. 2, displays very different behavior. Initially (a), we observe a morphology that is similar to that of the Newtonian fluid, i.e., viscoelasticity is negligible at first. As the thinning progresses, the polymeric fluid develops a longer neck with a

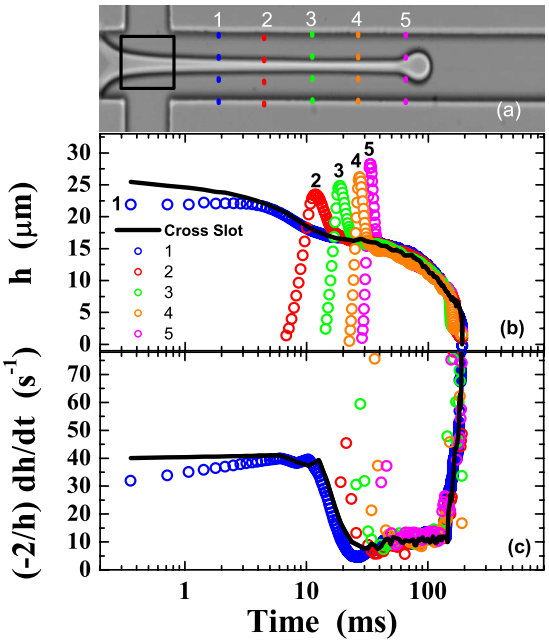

FIG. 3. (Color online) Position independence of the measurement. (a) Filament thickness $h(t)$ measured at different locations in the microchannel. Measurements are performed in the cross-slot region (solid line box) and at (dashed lines) 1, 2, 3, 4, and 5 channel widths downstream from that point. (b) The filament thickness for the polymeric fluid at $q=60$ measured at different positions. Data is color coded according to (a). (c) The computed extensional strain rate $\dot{\varepsilon}$ for the same cases shown in (b). The data shows that the measurements of $h(t)$ are nearly independent of axial position, after an initial transient.

drop attached to it (b). This filament elongates while thinning at a slower rate than in the Newtonian case (c). Near the breakup event, the polymeric fluid shows multiple beads ("beads-on-a-string") attached to the filament (d) [8,10,21]. After breakup, there are many satellite drops (e).

B. Quantitative

The filament thinning process is quantified by the decrease in diameter $h(t)$ as a function of time. To accomplish this, we fit a third-order polynomial equation to the interface contour, which is restricted to the cross-slot region. The field of view corresponding to the cross-slot region, in which $h(t)$ measurements are performed, is delimited by the solid line rectangle shown in Fig. 3(a). We assume that the interface is symmetric across the centerline and only half of the contour is fitted with the polynomial. We then locate the absolute value of the minimum in the polynomial first derivative. The filament diameter is measured at the point where the absolute value of the minimum in the first derivative is located. There are instances, however, where the minimum in absolute slope may be located at the edge of the cross-slot region. Hence we must check the dependence of $h(t)$ on measurement location, i.e., axial position z.

We test the dependence of $h(t)$ on axial position z by measuring $h(t)$ in the cross-slot region and also 1, 2, 3, 4, and 5 channel widths downstream from the edge of the cross-slot region [Fig. 3(a)]. Results are presented in Fig. 3(b); the values of $h(t)$ measured at different locations in the channel are nearly the same except for an initial transient. It follows that the values of the extensional strain rate $\dot{\varepsilon}$ [Fig. 3(c)] measured at different locations are also very similar. Here, we assume that $\dot{\varepsilon}=-(2/h)dh/dt$. We will check the validity of this assumption next.

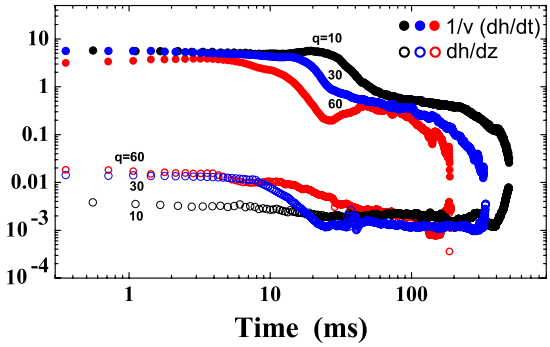

FIG. 4. (Color online) Filament axial spatial gradient dh/dz and normalized extensional strain rate $(1/v)dh/dt$ as a function of time for a polymeric fluid filament. Here, v is the average velocity inside the fluid filament. Measurements are performed for different flow rate ratios $q=10$, 30, and 60. The data shows that $dh/dz \ll (1/v)dh/dt$ so filament thickness spatial gradients may be neglected when computing the extensional strain rate $\dot{\varepsilon}$.

The extensional strain rate can be assumed to be $\dot{\varepsilon}=-(2/h)dh/dt$ only if the filament thickness h is homogeneous in the axial coordinate z [22,23]. However, there is some variation with z and an extra term in the extensional strain rate that is proportional to (dh/dz) may arise. In order to check whether this extra term can be neglected (or not), we consider an argument based on dimensional analysis: to convert $(v/h)(dh/dz)$ to a strain rate requires an inverse time scale, which must be given by a speed over a length. The only speeds in the system are v and dh/dt. Here, v is the average fluid velocity inside the filament, which is much larger than dh/dt. The only lengths in the system are h and the channel width, W; the former is smaller. Therefore the biggest possible extra term in the extensional strain rate $\dot{\varepsilon}$ would be a constant times $(v/h)(dh/dz)$.

Following the argument above, we compare the space and time derivatives (Fig. 4). We express them nondimensionally as dh/dz and $(1/v)dh/dt$, where the prefactor $(1/v)$ makes the time derivative dimensionless. We find that the space derivative of the filament thickness is at least an order of magnitude smaller than the dimensionless time derivative. Hence the extensional strain rate can be safely assumed to be $\dot{\varepsilon}=-(2/h)dh/dt$.

To summarize, the results in Figs. 3 and 4 show that one can, to a good approximation, study the thinning process by treating the filament as if it is nearly uniform spatially, with a thickness that depends only on time.

IV. RESULTS

A. Flow-driven regime

In Fig. 5(a), we present sample results of measurements of filament thickness $h(t)$, performed in the cross-slot region,

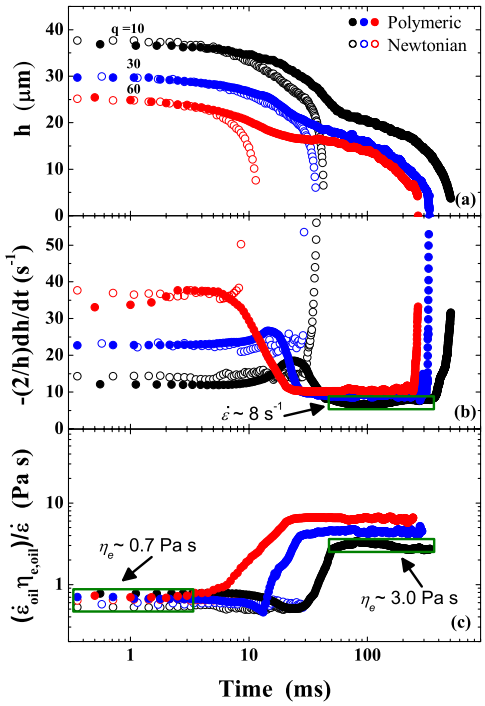

FIG. 5. (Color online) Time-dependent filament thinning. (a) Filament thickness $h(t)$ for both Newtonian and polymeric fluids for $q=10$, 30, and 60. (b) Filament extensional strain rate $\dot{\varepsilon}=-(2/h)dh/dt$ for the same fluids. Both viscous and elastic regimes are characterized by constant $\dot{\varepsilon}$. The value of $\dot{\varepsilon}$ is equal to 8 s^{-1} for a polymeric fluid at $q=10$. (c) The quantity $(\dot{\varepsilon}_{oil}\eta_{e,oil})/\dot{\varepsilon}$ is the filament extensional viscosity η_e where the flow is extensional, i.e., $\dot{\varepsilon}=$const. Here, $\dot{\varepsilon}_{oil}$ and $\eta_{e,oil}$ are the oil extensional strain rate and extensional viscosity, respectively. Initially, for all fluids, the values of η_e are similar since all fluids have nearly the same η_s. Later, the steady-state value of η_e increases with larger values of q.

as a function of time. We show data for both Newtonian and polymeric fluids for three flow rate ratios, $q=10$, 30, and 60. At short times, the Newtonian and polymeric fluids exhibit identical initial thinning, which is indicative of their common η_s; but at longer times, the two diverge with the polymeric filament lasting at least an order of magnitude longer before breakup. We also note shorter breakup times as q is increased. This trend is also found in other flow-focusing experiments [2,24] and in a numerical investigation [25] using Newtonian fluids.

The filament extensional strain rate $\dot{\varepsilon}=-(2/h)dh/dt$ is shown as a function of time for the same flow rate ratios q, in Fig. 5(b). For the Newtonian fluid, $\dot{\varepsilon}$ is initially independent of time; therefore, in this regime, $h(t)$ decreases exponentially with time. For the polymeric fluid, $\dot{\varepsilon}$ is initially equal to the same constant as for the Newtonian fluid; but it soon departs and, after a transient interval, settles down to smaller constant value, which indicates a second regime of slower exponential thinning. For all fluids at the very latest times, close to breakup, the final decrease of $h(t)$ to zero gives an apparent divergence of $\dot{\varepsilon}$. We show in Sec. IV B that the data just before breakup are consistent with a linear decrease in filament diameter, $h(t)\propto(t-t_b)$ where t_b is the breakup time.

To model the exponential decrease of filament diameter, we assume that (1) filament thinning is driven mainly by the outer fluid extensional flow in the cross-slot region and (2) the shear flow that develops is relatively far downstream from the cross-slot region and should have no implications on the local stress balance. These are reasonable assumptions since shear stresses tangential to the filament do not contribute to the thinning (or squeezing) of the filament; filament thinning is driven by outer fluid (oil) viscous stresses normal to the filament.

Starting from an assumption of stress balance inside and outside the interface, and applying the definition of extensional viscosity [19], we obtain the condition $\eta_e\dot{\varepsilon}=\eta_{e,oil}\dot{\varepsilon}_{oil}$, which relates the strain rates and extensional viscosities of the inner and outer phases. Here, the left and right sides are the extensional viscosity multiplied by the extensional strain rate for the aqueous filament and continuous oil phases, respectively. As discussed above, the strain rate in the filament is $\dot{\varepsilon}=-(2/h)dh/dt$. The strain rate for oil in the cross-slot region is $\dot{\varepsilon}_{oil}\approx Q_{oil}/(W^2L)$, as verified by particle-tracking methods [26]. Lastly, since the oil is Newtonian, its extensional viscosity is $\eta_{e,oil}=3\eta_{s,oil}$, where $\eta_{s,oil}$ is the oil shear rate viscosity [19,27]. Therefore also assuming that η_e is independent of time, the filament diameter thins exponentially according to

$$h(t)=h_o\exp[-(3/2)(\eta_{s,oil}/\eta_e)\dot{\varepsilon}_{oil}t]. \quad (1)$$

where h_o is an integration constant. This equation is valid for the two flow-driven exponential regimes shown in Fig. 5. In such *flow-driven* regimes, Eq. (1) may be used to deduce η_e from $h(t)$ data.

We note that the quantity $\dot{\varepsilon}_{oil}$ is measured in the cross-slot region, where the flow is extensional and where pinching from the "mother drop" occurs. To this end, we have checked that $\dot{\varepsilon}_{oil}$ remains constant during the filament thinning and breakup event; the average velocity of the oil in the cross-slot region is constant.

The transition between the two exponential thinning regimes can be elucidated by plotting the quantity $\varphi=(\dot{\varepsilon}_{oil}\eta_{e,oil})/\dot{\varepsilon}$, which has units of viscosity, as a function of time [Fig. 5(c)]. We find that φ is nearly constant in regions where $\dot{\varepsilon}$ is constant. In such regions, the quantity φ is the same as the filament extensional viscosity η_e.

The values of η_e are computed for each steady extensional strain-rate $\dot{\varepsilon}$, which is proportional to q, as shown in Fig. 5(c). We find that (i) the initial value of η_e is independent of q and (ii) the steady-state value of η_e increases as the flow rate ratio q is increased.

B. Capillary-driven regime

The linear decrease of the filament thickness near the final breakup can also be modeled by stress balance, now by incorporating surface tension effects. Specifically, the Rayleigh-plateau instability eventually sets in so that capillary forces cause beading and ultimately breakup. Equating radial stress with the Laplace pressure gives $\eta_e\dot{\varepsilon}=\sigma/h$ [7,28,29]. Therefore the filament diameter thins linearly with time according to

$$h(t)=-(1/2)(\sigma/\eta_e)(t-t_b), \quad (2)$$

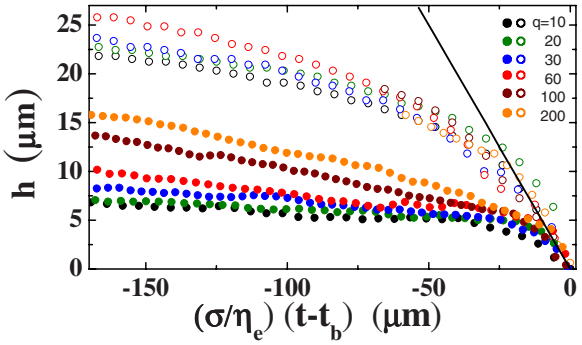

FIG. 6. (Color online) Filament thickness versus time in the capillary driven regime, where t_b is the breakup time. At very late times, the filament thins roughly linearly in time with a speed proportional to σ/η_e for both Newtonian (open circles) and polymeric (closed circles) fluids. The flow ratio (q) is color-coded in the legend for both cases. The solid line represents slope=−1/2.

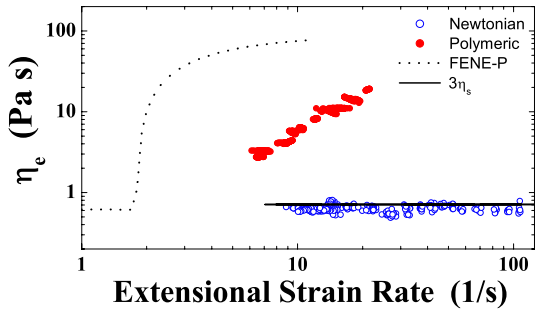

FIG. 7. (Color online) Extensional viscosities of both Newtonian and polymeric fluids, derived from the filament thinning measurements and Eq. (1), as a function of the extensional strain rate $\dot{\varepsilon}=-2/h(dh/dt)$. The polymeric fluid extensional viscosity shows strain-rate thickening behavior and increases with a power law exponent of approximately 1.0. The theoretical Trouton ratio of a Newtonian fluid is 3.0 (solid line). The FENE-P model prediction is also shown, but is far from the measurements.

where t_b is the breakup time. In such *capillary-driven* regimes, Eq. (2) may be used to deduce η_e from $h(t)$ data. Equation (2) shows that, near the singularity, $h(t)$ varies linearly with $(t-t_b)$ with slope $\sigma/2\eta_e$, which has been observed numerically [30] in the Stokes regime, except that, in the numerical work, shear rather than extensional viscosity is used in the denominator. A linear regime has also been observed numerically for polymeric solutions near the final breakup [12,31].

To demonstrate the consistency of our extensional viscosity results in the flow- and capillary-driven regimes, we plot data for $h(t)$ vs $(\sigma/\eta_e)(t-t_b)$ in Fig. 6. There, the value of η_e is taken from analysis of the flow-driven regime using Eq. (1). To within apparently random deviations, the $h(t)$ data vanish linearly with $(\sigma/\eta_e)(t-t_b)$ with slope $-1/2$, in accord with Eq. (2). Note, however, that the dynamic range is limited, since the imaging resolution is about 2 μm. Therefore the capillary-driven regime is consistent with the flow-driven regime, but the latter gives more accurate values of extensional viscosity η_e.

V. DISCUSSION

The extensional properties of polymeric fluids are important for applications such as turbulent drag reduction and splash suppression [19,32]. However, measurement of η_e has remained a difficult task [33]. We now show that high-quality data on the values of steady extensional viscosity for both polymeric and Newtonian fluids can be obtained using our method.

Final results for η_e based on Eq. (1) are plotted in Fig. 7 vs extensional strain rate. Here each point represents a different fixed flow-rate ratio, q. For the Newtonian fluid, η_e is independent of extensional strain rate and nearly equals $3\eta_s$ as expected [19,27]. This agreement serves as a second check, complementary to Fig. 6. For the polymeric fluid at early times, in the first flow-driven regime, the behavior is the same as for the Newtonian fluid (not shown). At later times, in the second flow-driven regime, the extensional strain rate of the filament is lower and η_e is higher. This "strain-rate thickening" behavior is due to the stretching of the polymer molecules in the extensional flow of the thinning filament and it has been observed in other macroscopic experiments [22,34].

It is important to point out that the values presented in Fig. 7 are for steady extensional viscosity and not transient extensional viscosity, which is usually reported in macroscopic experiments [22,34]. Here, values of η_e are computed for each steady extensional strain-rate $\dot{\varepsilon}$, which is proportional to q, as shown in Figs. 5(c) and 7.

In Fig. 1, the FENE-P model properly describes both the η_s and N_1 versus shear rate with two adjustable parameters, which are $\lambda=0.45$ s and $b=4500$. An expression for η_e can be obtained from the FENE-P model for a range of extensional strain rates [18,20] using the values of λ, b, and $\eta_{s,solv}$. The FENE-P prediction for η_e is plotted in Fig. 7. It exhibits strain-rate thickening behavior, which saturates at high strain rates by accounting for the finite extensibility of the polymer molecules. However, by comparison with our data, the predicted strain-rate thickening sets in too soon and too abruptly. A possible source of error in the model may be polymer dispersivity (~15% in M_W), which can smear out the sharp rise in η_e [9]. It cannot, however, account for such early transition to strain-rate thickening behavior since $\lambda \sim M_W^{3/2}$.

Other sources of error may be the inherent limitations of the FENE-P model such as the averaging of the force values connecting the beads in the dumbbell model originally proposed by Peterlin [17]. This averaging is known to lead to unexpectedly large polymeric stresses compared to the non-averaged FENE model [35]. Another limitation is that while real polymeric fluids have a spectrum of λ, the FENE-P model, as used here, is described by a mean λ obtained in a shear flow, which is known to be low for use in extensional flows. Therefore we should expect some type of failure of predictions of η_e based on the single mode FENE-P model. This disagreement does not imply a weakness in the measurement.

VI. CONCLUSION

In conclusion, small amounts of flexible polymer can dramatically affect filament thinning and breakup in microchannel extensional flow. We find both a *flow-driven* regime in which the filament thins followed by a *capillary-driven* regime responsible for filament breakup. For a Newtonian fluid, the filament thins exponentially with time until onset of capillary surface tension-induced breakup. For the polymeric fluid with the same shear viscosity (nearly independent of shear strain rate), there is an intermediate regime in which the filament thins exponentially at a much slower rate. Furthermore, in the capillary regime a series of small droplets is generated along the filament. These differences may be attributed solely to extensional viscosity and its increase with extensional strain rate, since this is the only rheological difference between the Newtonian and polymeric fluids. For thinner filaments and faster thinning, the polymer molecules stretch and cause an increase in extensional viscosity without significant change in shear viscosity. Further, for polymeric fluids, the crossover from flow-driven to capillary-driven regime may depend on the elastocapillary number EC $=\mathrm{De}/\mathrm{Ca}=\lambda\sigma/(\dot{\varepsilon}L)$, where De is the Deborah number. This suggests that the crossover depends on the system length scale L.

Measurements of the exponential rate of thinning can thus be used to determine the steady extensional viscosity, an elusive quantity to measure. For the Newtonian case, $\eta_e \approx 3\eta_s$; for the polymeric case, the values of η_e increase with extensional strain rate, but much more slowly than predicted by the FENE-P model. This suggests the need for a better understanding of both the molecule-scale behavior of polymers in extensional flows as well as its connection to macroscopic rheology. Filament thinning in microchannels, and its variations with polymer molecular weight, may be a promising approach.

ACKNOWLEDGMENTS

We thank Gareth McKinley, who provided many insightful comments to the paper. We also thank Daniel Bonn and Howard Stone for fruitful discussions. Seth Fraden and Katie Humphry provided help with microfabrication methods. Kerstin Nordstrom and Ben Polak assisted with experiments. This work was supported by the National Science Foundation through Grant No. MRSEC/DMR05-20020.

[1] J. Eggers, Rev. Mod. Phys. **69**, 865 (1997).
[2] S. Anna, N. Bontoux, and H. Stone, Appl. Phys. Lett. **82**, 364 (2003).
[3] R. Dreyfus, P. Tabeling, and H. Willaime, Phys. Rev. Lett. **90**, 144505 (2003).
[4] J. Gordillo, Z. Cheng, A. Ganan-Calvo, M. Marquez, and D. Weitz, Phys. Fluids **16**, 2828 (2004).
[5] P. Garstecki, I. Gitlin, W. DiLuzio, G. Whitesides, E. Kumacheva, and H. Stone, Appl. Phys. Lett. **85**, 2649 (2004).
[6] D. R. Link, S. L. Anna, D. A. Weitz, and H. A. Stone, Phys. Rev. Lett. **92**, 054503 (2004).
[7] P. Garstecki, H. A. Stone, and G. M. Whitesides, Phys. Rev. Lett. **94**, 164501 (2005).
[8] M. Goldin, J. Yerushal, R. Pfeffer, and R. Shinnar, J. Fluid Mech. **38**, 689 (1969).
[9] C. Wagner, Y. Amarouchene, D. Bonn, and J. Eggers, Phys. Rev. Lett. **95**, 164504 (2005).
[10] C. Clasen, J. Eggers, M. Fontelos, J. Li, and G. McKinley, J. Fluid Mech. **556**, 283 (2006).
[11] V. Tirtaatmadja, G. McKinley, and J. Cooper-White, Phys. Fluids **18**, 043101 (2006).
[12] V. Entov and E. Hinch, J. Non-Newtonian Fluid Mech. **72**, 31 (1997).
[13] C. Zhou, P. Yue, and J. Feng, Phys. Fluids **18**, 092105 (2006).
[14] J. Husny and J. Cooper-White, J. Non-Newtonian Fluid Mech. **137**, 121 (2006).
[15] S. Quake and A. Scherer, Science **290**, 1536 (2000).
[16] S. Sia and G. Whitesides, Electrophoresis **24**, 3563 (2003).
[17] A. Peterlin, J. Polym. Sci., Part B: Polym. Lett. **4**, 287 (1966).
[18] R. Bird, C. Curtiss, R. Armstrong, and O. Hassager, *Dynamics of Polymeric Liquids: Fluid Mechanics*, Vol. 1, 2nd ed. (Wiley, New York, 1987).
[19] G. McKinley and T. Sridhar, Annu. Rev. Fluid Mech. **34**, 375 (2002).
[20] A. Lindner, J. Vermant, and D. Bonn, Physica A **319**, 125 (2003).
[21] H. Chang, E. Demekhin, and E. Kalaidin, Phys. Fluids **11**, 1717 (1999).
[22] Y. Amarouchene, D. Bonn, J. Meunier, and H. Kellay, Phys. Rev. Lett. **86**, 3558 (2001).
[23] M. Oliveira and G. McKinley, Phys. Fluids **17**, 071704 (2005).
[24] T. Thorsen, R. W. Roberts, F. H. Arnold, and S. R. Quake, Phys. Rev. Lett. **86**, 4163 (2001).
[25] D. Zhang and H. A. Stone, Phys. Fluids **9**, 2234 (1997).
[26] P. E. Arratia, C. C. Thomas, J. Diorio, and J. P. Gollub, Phys. Rev. Lett. **96**, 144502 (2006).
[27] F. Trouton, Proc. R. Soc. London, Ser. A **77**, 426440 (1906).
[28] I. Cohen, M. P. Brenner, J. Eggers, and S. R. Nagel, Phys. Rev. Lett. **83**, 1147 (1999).
[29] W. W. Zhang and J. R. Lister, Phys. Rev. Lett. **83**, 1151 (1999).
[30] J. Lister and H. Stone, Phys. Fluids **10**, 2758 (1998).
[31] M. Fontelos and J. Li, J. Non-Newtonian Fluid Mech. **118**, 1 (2004).
[32] V. Bergeron, D. Bonn, J. Martin, and L. Vovelle, Nature (London) **405**, 772 (2000).
[33] S. Anna, G. McKinley, D. Nguyen, T. Sridhar, S. Muller, J. Huang, and D. James, J. Rheol. **45**, 83 (2001).
[34] S. Anna and G. McKinley, J. Rheol. **45**, 115 (2001).
[35] A. van Heel, M. Hulsen, and B. van den Brule, J. Non-Newtonian Fluid Mech. **75**, 253 (1998).